ISSN: 2755-631X

Research Article

Journal of Global Health and Social Medicine

Assessment of Pollutant Emissions and Combustion Efficiency due to Inserting Aerodynamic Solid Body in High-Temperature Flame Regions

Anvar Ahmadkhah

PhD of mechanical engineering, Iran University of Science and Technology, Iran

Corresponding author
Anvar Ahmadkhah, PhD of mechanical engineering, Iran University of Science and Technology, Iran.

Received: July 21, 2025; **Accepted:** August 06, 2025; **Published:** August 15, 2025

ABSTRACT
This study evaluates a method of using a solid body with a special aerodynamic shape to redistribute the burner's peak temperature region in the flame. This method extends the low-temperature range and suppresses thermal nitric oxide formation by numerical simulation. The model used for this purpose is a 7-fin fan blade with a bluff body for generating the wake region downstream of the cylindrical combustion chamber. The results are validated using the static temperature reported in the published paper for the burner without inserting a solid body in the flame region. There was a good agreement between experimental data and those calculated by applying the model for industrial application. The results cover the fin blades' axial distance and fins' axial length parameters in the wake region. Also, the right fins' axial distance and axial length in the downstream combustion flow were calculated by extracting the maximum axial length of the wake region. The burner's efficiency improved by 2.5% when installing a solid body burner. Moreover, NOx emission was investigated for 130 cases of numerical models related to the fins' axial length and axial distance parameters. The results indicated a decrease of 33.6% in NOx parts per million value, which was calculated for the selected inserting solid body burner in the flame region.

Keywords: Numerical Simulation, In-Flame Fin Insertion, NOx Reduction, Combustion, Burner

Introduction

The current quality outline has been considered an effective and tenable alternative for strength creation and alleviation of contaminant emissions in exhaustive industries. In recent ages, waste heat improvement and waste stream fixed price as fuels have been presented as hopeful substitutes for reconstructing the effectiveness of result processes[1,2].

Combustion processes are among the main determinants for air contaminants such as NOx, SO2, and articulate matter [3]. NOx is caused during the combustion process in an extreme heat domain(Nabi, 2010) and is known as a source of big air dirtiness that produces gases forming the atmosphere when it reacts with light for 24 hours 5].

Thermodynamics, action, and transport phenomena are strongly mixed training in the combustion process. These features may be expressed mathematically using the fundamental bulk, impetus, and energy preservation equations [6].

The new combustion systems will be needed in industry using energy resources and the environment. Special expertise with affordable prices is required for designing these new combustion systems. Computational Fluid Dynamics (CFD) is a highly useful approach to overcome the costs of exploratory tests. The CFD method is very effective and spans a range of technical and non-mechanical request areas and large-scale combustion applications. Increased CPU cost demands are due to model specifications and a large span of scales in the geometry [7].

The CFD method has been confirmed to be a very beneficial tool for supplying valuable facts about the operating processes in furnaces [8]. Numerous new flamelet models have been developed and investigated since Peters introduced the original flamelet model [9-13]. The turbulent non-premixed hydrogen and hydrocarbon flames are studied through numerical simulation [14]. Employing CFD modeling as a major engineering design

Citation: Anvar Ahmadkhah. Assessment of Pollutant Emissions and Combustion Efficiency due to Inserting Aerodynamic Solid Body in High-Temperature Flame Regions. J Glob Health Soci Med. 2025. 1(2): 1-9. DOI: doi.org/10.61440/JGHSM.2025.v1.12

tool for burners reduces time to market [15]. In particular, it enables recent progress in high-performance computing to simulate high levels of complexity of burner geometries [16,17].

Based on the mentioned points, this research proposes a numerical study of the effects of inserting the aerodynamic solid body fin shape. The variables used in this model are the fins' axial length and fins axial distance from the flame in combustion distribution and combustion effect. The advantage of this method is that it is possible to calculate many combustion parameters that are not possible with experimental methods. In this respect, placing the sensor in the flow field that experimentally measures the fluid parameters will affect the fluid flow field, and the validity of the results will be far from the real state [18,19].

Accordingly, the fluid flow, temperature field distribution, efficiency, and NOx are explored to judge the effect of its combustion through ANSYS Workbench software simulation. The research results have certain reference values for the combustion distribution of gas burners by inserting aerodynamic solid bodies in the field of gas burners [20].

Method

This study investigates the application of a solid body through the 3D numerical simulation of the flame temperature field compared to the ordinary combustion chambers' temperature field. This technique depends on using an aerodynamic solid body with a symmetrical cross-section shape in the flame region of the combustion chamber. The aerodynamics of a solid body redistribute flame temperatures to reduce thermal no-formation. This method aims to decrease the peak temperature and suppress the thermal nitric oxide formation concerning the normal combustion process. In the numerical model, the downstream of the cylindrical test section is equipped with the 7 fin fan blades and the bluff body for generating the wake region. The geometry of the solid model body used in the fluid combustion flow field is in the form of 7 fin fan blades with constant thickness, which are located around the center of a circle. These 7 fin fan blades are placed in the flow field such that their longitudinal axis is along the central axis of the combustion chamber. Also, they are placed in the flow field after the bluff body and wake region. The computational model of the combustion chamber, bluff body, and fin fan blade was set up in the commercial CFD tool of ANSYS Fluent using its built-in sub-models and algorithms. In the numerical models used for this research, the length of the symmetric 7-fin fan blades is variable. The distance from the bluff body is another parameter included in the analysis of the results of their effects. A total of 130 numerical models in three-dimensional mode and with defined variables are used in numerical analysis. The numerical results of efficiency, NOx parts per million (ppm), the mass average of the rate of thermal NOx, the mass average of the rate of prompt NOx, and molar concentration were compared with those for a normal combustion chamber.

Model for CFD Simulation

Figure. 1 illustrates a burner model with the bluff body dimensions and 7 fan blades used in numerical simulation. The axis of the conical bluff body with a blockage ratio of 0.6 and 45°C angle is located at the end of the premixed cylindrical region with a diameter of 80 mm for stabilizing the flame and preventing the flashback at high air temperature. A total of 7 fin fan blades with a thickness of 2 mm and variable axial length are located downstream of the test section and behind the wake region generated by the conical bluff body during the combustion process. The axial position of the fin fan blade is variable to find a suitable distance so as not to disturb the wake region in the combustion process. Figure. 1(a) presents the dimensions of the test section with a bluff body and 7 fin fan blades. Also, Figure. 1(b) provides the 3D isometric view of the burner and the location of the bluff body with fin fans.

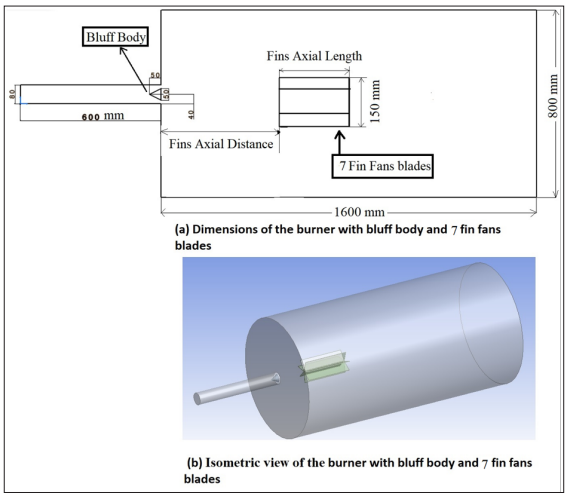

Figure 1: Model of the burner with a bluff body and fin fan blades: (a) burner with the dimensions of the bluff body and 7 fin fan blades and (b) Isometric view of the burner

The computational model of the combustion chamber was set up using the ANSYS Fluent software simulation tool. The fluid domain of the present study was simulated based on the premixed gaseous burner. A conical bluff body is used in numerical simulation to stabilize the flame. The premixed gaseous through the inlet of the burner with constant velocity magnitude is used in the CFD domain. Figure. 2 illustrates the 3D mesh generated for the burner system. The numerical fluid domain, including the bluff body and 7 fin fan blades, was mesh generated using the hexahedron-type volumetric element. Here, the number of volumetric elements was 1870464. The single block fluid mesh had a curvature size function with good cell quality specifications (0.25-0.71). The element shape was checked using the common measuring method based on the equivalent angle skewness, and the mesh quality parameters could be viewed as graphs. Figure. 2(a) shows a 3D mesh with boundary conditions used in numerical simulations. Figure. 2(b) demonstrates the grid used near the bluff body region. The mesh with excellent cell quality (0-0.25) was employed to capture all the relevant flow features behind the bluff body. The outcomes were validated by checking mesh independence. Figures. 2(c) and 2(d) show the structural grid used in the burner's inlet and multi-block grid outlet.

Predicting the combustion process was more complex with heat transfer calculation from the wall. This process includes the treatment of phenomena such as free convection, conduction, and radiation, most of which were covered in this study. All the walls are set to no-slip adiabatic walls. When defining thermal conditions for the wall of the combustion chamber and the wall of the premixed tube, the thermal boundary conditions are as follows:

$$q = 0 \quad (1)$$

where q is the heat flux at the surface of the walls. The outlet boundary condition is set to atmospheric pressure.

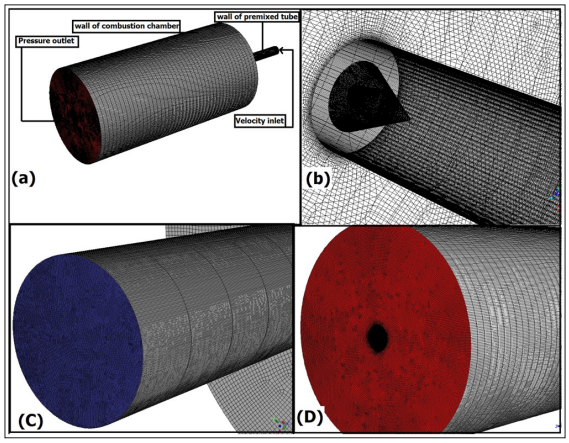

Figure 2: A three-dimensional (3D) mesh-generated burner system: (a) 3D of the burner system with boundary conditions, (b) grid used near the bluff body region, (c) structural grid used in the inlet of the burner, and (d) multi-block grid in the outlet domain in the burner

The lack of comprehensive experimental data on the issues motivated us to validate the present work by comparing the published experimental research results. The combustion simulation for the burner without inserting a model of solid fins was performed in ANSYS FLUEN using κ-ε (turbulence) and eddy-dissipation (chemistry) models in steady-state conditions [21]. The pressure-based solver was used without any radiation mechanism for the walls and propane-air mixture materials. The solution method enabled the pressure-velocity coupling, and the gradient used least square-cell based. Turbulence kinetic energy, turbulence dissipation rate, and energy order upwind were used for pressure. The boundary condition of the bluff body and fins blades was adiabatic, and the no-slip condition was under free slip condition. Figure. 3 illustrates the full view of the 3D numerical domain and the location of the middle cross-section plane using static temperature contour in the middle cross-section plane of the burner CFD domain. Also, the color spectrum of predicted static temperatures and the location of temperature changes are shown on the two-dimensional cross-section relative to the coordinate axes Y-Z.

Figure. 4 compares the findings of the studies and published experimental results in axial distance measured in a line parallel to the flame centerline. The static temperature reported in the published paper by Abdelaal [22] was used for the burner without inserting a solid body to show the validity of using a finite volume model. Abdelaal reported an acceptable agreement between the results of the studies. Also, the exact mismatch of the temperature points in the results is because temperature measuring props are used to experimentally measure the temperatures in the desired points. Meanwhile, the temperature sensor's placement will cause very small changes in the flow temperature field.

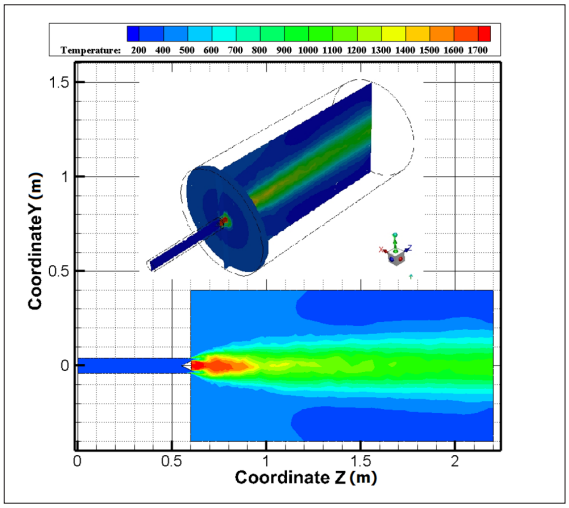

Figure 3: The static temperature contour in the middle cross-section plane of the burner CFD domain

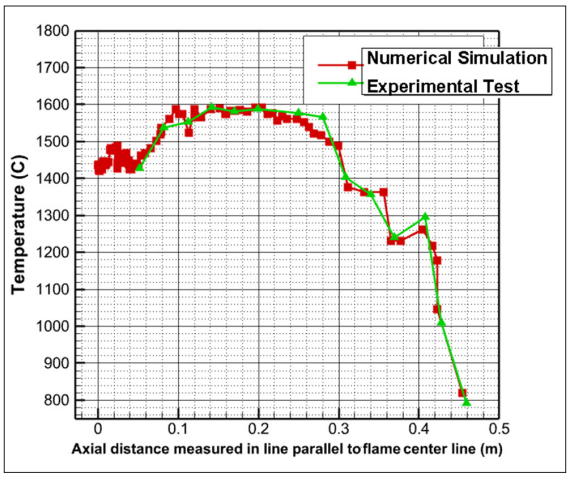

Figure 4: The curve of static temperature profile for burner studied by Abdelaal [22]. red solid line: Current model; green dotted line: results of Abdelaal [22].

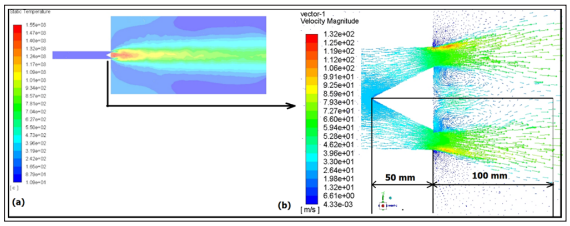

Figure 5: Static temperature contour and the vortex field (wake region): (a) Static temperature contour in the middle cross-section plane of the burner CFD domain and (b) vortex field (wake region) behind the bluff body in the middle cross-section plane of the burner CFD domain

Figure. 5 shows the static temperature contour and the vortex field (wake region) produced after the bluff body in the middle cross-section plane of the burner CFD domain [23]. Generally, inflow temperature and oxygen content affect the vortex shedding, flame vortex interaction, vortex structure, and the magnitude of the vortex formed in the wake region [24]. Figure. 5(a) shows the high gradient temperature behind the bluff body in numerical simulation. According to Figure. 5(b), the maximum axial distance along the centerline for the wake region is 100

mm. This length is important for finding the best start location for inserting 7 fin fan blades in the direction of the centerline in the burner CFD domain.

Based on Figure. 5, it is found that downstream of the combustion fluid field, the maximum axial distance along the centerline for the wake area region of the stream is 10 cm. Combustion flow has a complex nature such that there is an interference of the flows between 7 fin fan blades and the bluff body. Therefore, the effects of different 7 fins fan blade lengths and the starting placement of the 7-fin fan blades in the direction of the centerline flow field were investigated through numerical simulation. In the present study, the parameter fin axial distance changes between 5 and 30 cm, and the parameter fin axial length changes between 20 and 45 cm. Overall, 130 premixed combustion case models have been made in 3D and numerically solved. The solution results are compared by considering the results of the model without inserting a solid body in numerical simulations. The results of the product composition of the burner without inserting a solid body for Nitrogen oxide concentration, Mass average of rate thermal no-formation, Mass average of rate prompt no-formation, and Molar concentration of N2 are presented in Table 1. The mass average results are calculated using the volume integral method in all of the 3D CFD domains. Also, Nitrogen oxide concentration and molar concentration of N2 are calculated using the surface integral method at the pressure outlet in the boundary of the control volume. In the following, the other models are evaluated using the product composition results from Table 1, with the burner inserted in the solid body.

Table 1: Results of calculations for the burner without inserting solid body.

Product Composition	Unit	Quantity
Nitrogen oxide concentration	(ppm)	48.17443
Mass average of rate thermal no-formation	*kg mole*/(m^3-*s*)	6.61E-6
Mass average of rate prompt no-formation	*kg mole*/(m^3-*s*)	6.369E-10
The molar concentration of N2	k mole/m^3	0.022

Results

Temperature Field

As mentioned in the modeling section, more than 130 burner cases with different fins axial lengths and fins axial distance geometries were numerically tested. The results were used to find the correct axial length and axial distance concerning the bluff body in the control volume of the burner to reach the final selection step. In this respect, the formation of thermal nitric oxides in normal combustion and 3D region shrinkage of the peak temperature with the flame middle medium in the lower range temperature (400 °C ton1300°C) are suitable issues. Therefore, the aim is to reduce the areas of the flow that have high-temperature values and lower the maximum peak temperature in the flow field by changing the fins' axial length from the bluff body and their axial distance. Among the contour of static temperature results, we selected the contour of Static temperature on a middle cross-section plane relative to different fins' axial lengths at the constant fin axial distance along the centerline (Figure. 6). As shown in Figures. 6(a), 6(b), and 6(c), by increasing the fins' axial length from 20 cm to 32.5 cm, the peak temperature values decreased from 2200°C to 1800°C. In addition, according to the previous result, the 3D region of high-temperature values around the fins model and near the burner walls gradually changed and decreased. Figures. 6(d), 6(e), and 6(f) show that at a constant fin axial distance of 7.5 cm and increasing the fin's axial length from 27.5 cm to 32.5 cm, the peak temperature value maintains its value around 1800°C. However, the high 3D gradient temperature region around the fins blade continues to decline with a sharper trend from 1800°C (red color in Figure. 6d) to 1560°C (Figure. 6f). In Figure. 6(e), the big part of the 3D region near the wall of the combustion chamber has a value of around 1500°C (with orange color) and a higher temperature region (with a light red color) in front of the fins blade at a 1650°C along the centerline.

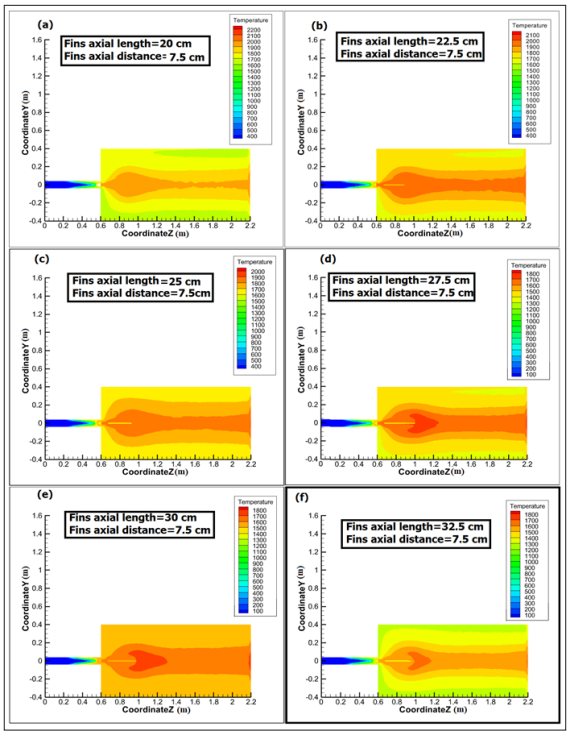

Figure 6: Static temperature contour on a middle cross-section plane relative to different Fins axial length

In Figure. 6(f), the temperature of the 3D region near the wall declines to 850°C. Also, the dimension of the 3D region of a high-temperature region with a light red color in front of the blade centerline becomes smaller with lower static temperature values equal to 1600°C. Based on these results, the appropriate choice for fin axial length is 32.5 cm, and the best installation position in the direction of the centerline in the burner is the distance of 7.5 cm from the end of the bluff body. Figure. 7 shows the contour of static temperature in the 3D CFD domain for the fins' axial length of 32.5 cm and fins' axial distance of 7.5 cm. Figure. 7(a) shows the contour of static temperature on a middle cross-section plane in the x and y direction. As can be seen, the flow field of the temperature and other parameters of the combustion fluid have a symmetrical pattern in the direction of the central axis in the downstream flow for all regions in the CFD domain. Figure. 7(b) shows the predicted gradient temperature values on the bluff body and inserting solid model in the CFD domain. The figure also presents the symmetrical behavior related to the downstream flow's central axis for all CFD domain regions.

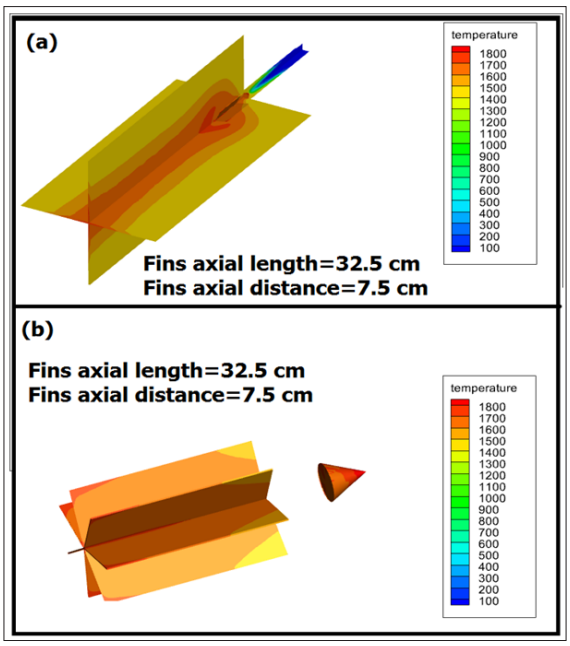

Figure 7: The contour of static temperature in the 3D CFD domain for fins axial length 32.5 cm and fins axial distance 7.5 cm: (a) contour of static temperature on a middle cross sections plane in x and y direction and (b) contour of static temperature on fins and bluff body solid model

Combustion Efficiency

Natural gas like PNG, LPG, and CNG are popular in the cooking and automobile industries. Generally, the burner with natural gas fuel has high combustion efficiency, often exceeding 90%. Calculation of combustion chamber efficiency changes concerning fin axial length. In this respect, the axial position is among the other parameters investigated in this article. This parameter is compared with the ordinary burner without inserting a solid body in the flame region. The heat transfer exchange between the walls of the combustion chamber and the surrounding environment is limited. Here, the efficiency of the combustion chamber is measured using the net heat flux at the pressure outlet, where it is possible to exchange heat with the outside environment. In our numerical model, it takes place through the exit of the combustion chamber. According to the quality of combustion and temperature changes in the flow field of the combustion chamber, the amount of heat lost through the outlet of the flow with the surrounding environment will vary with the fin axial length and fin axial distance from the bluff body. The combustion efficiency is calculated by deducting the flue gas heat losses from the maximum achievable 100% heat generated by the burner. The heat loss from the combustion chamber's exit occurs in the burner. Accordingly, the efficiency of the combustion chamber can be calculated the efficiency of the combustion chamber is determined by calculating the percentage of the output heat compared to the heat produced. Figure. 8 depicts the results of the efficiency calculations for this cylindrical combustion chamber concerning two variable parameters: fin axial distance and fin axial length along the flame centerline. The efficiency of the combustion chamber for the state in the combustion chamber without inserting a solid body is calculated using the same method. In this case, the efficiency of the combustion chamber is equal to 97.85%. Figure. 8 exhibits the efficiency of the combustion chamber for all inserting solid bodies related to the fin's axial length and fin's axial distance. In Figure. 8(a), the fin axial distance changes between 5 and 30 cm, and the fin axial length varies between 21 and 45 cm. In Figure. 8(b), fin fans with this particular aerodynamic shape are placed in the combustion flow field and within the numerical range of the specified parameters. As can be seen, this configuration has increased the efficiency of the combustion chamber compared to the combustion chamber without inserting a solid body. The burner's minimum efficiency is 98.2% when inserting a solid body. The efficiency of the combustion chamber for inserting a solid body with an axial fin length of 32.5 cm and fin axial distance of 7.5 cm is 99.745%, which is a good value but not the maximum value. Moreover, the highest efficiency of the combustion chamber was extracted for the case where the fin's axial length is equal to 27.5 cm, and its axial distance is 7.5 cm. In this case, the efficiency of the combustion chamber is equal to 99.745 percent, which is the maximum value among all models.

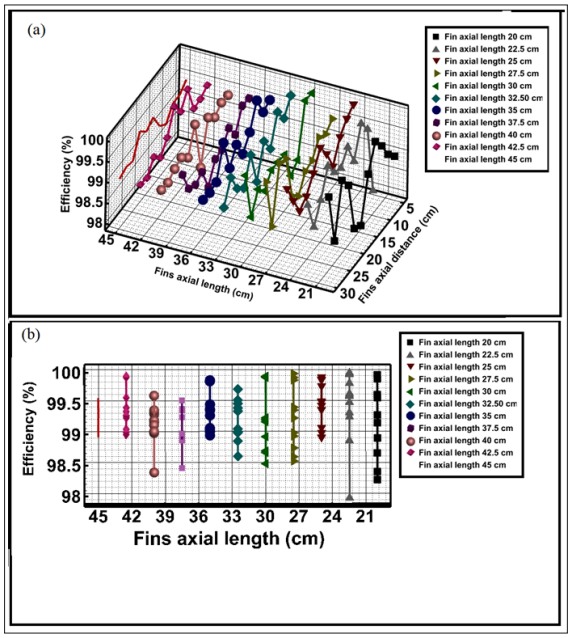

Figure 8: The result of the efficiency calculation is relative to variable fin axial distance and fin axial length: (a) Results of the Efficiency relative to two variables and (b) Result of the Efficiency relative to fins axial length

NOx Formation During the Combustion Process

Nitrogen oxides are the most common contaminants in nature. The nitric group of chemical elements (NO) and nitrogen dioxides (NO_2) are the principal nitrogen oxides in the climate and are usually referred to as NOX and inhaled anesthetic (N2O) [25-27]. Typically, NO is generated inside the reaction region, and the concluding corrosion of NO_2 occurs in a post-burn process out of the combustion domain [28-30]. Four main NO beginnings are caused in the burning process: thermal NO or Zeldovich system, prompt NO or Fennimore machine, fuel NO, and N2O. The main physiognomy of each NO composition system is debated in the following division [31].

The generation of thermal NO is consistent with the direct oxidation of nitrogen fragments. The three principal backlashes

of the thermal NO composition means are expressed as follows:

$N_2+O_2 \leftrightarrow NO+N$ (2)

$N+O_2 \leftrightarrow NO+N$ (3)

$N+OH \leftrightarrow NO+H$ (4)

Thermal NO or Zeldovich system is created throughout the combustion process. Eqs. (2) and (3) show that N_2 and O_2 form the chain reproducing steps known as the Zeldovich machine. The rate confining response in NO composition is the $N_2+O \leftrightarrow NO+N$ backlash. Thermal NO is very weak on hot nesses above 1500°C. The formation rate promptly increases, increasing the temperature due to extreme separation energy [32,33].

Figure. 9 shows the mass average of the rate of thermal no-formation in the entire burner control volume due to the heat accumulation related to the variable fins' axial length and its axial distance from the bluff body in all of the 3D CFD domains. Also, the high-temperature environment promotes the thermal no-formation. According to Figure. 9(a), the low no-formation rate (1.7E-09 - 4.47E-06) *kg mole*/(m^3-*s*) is calculated for burners with fins axial distance smaller than 10 cm and fins axial length lower than 35 cm. This observation is in agreement with the temperature distribution results in Figure. 6. The minimum formation rate for thermal NOx appears near the wall of the burner. By closing the wall fins along the centerline, thermal NOx formation increased gradually due to the high-temperature gradient (Fu et al., 2020). For the burner without inserting fin blades, the value of the mass average of the rate of thermal no-formation is 6.61E-06 *kg mole*/(m^3-*s*). Meanwhile, for the burner model with fin axial length is 32.5 cm and the fin axial distance is 7.5 cm. As shown in Figure. 9(b), the mass average of the rate of thermal no-formation is decreased to 2.88E-07 *g mole*/(m^3-*s*).

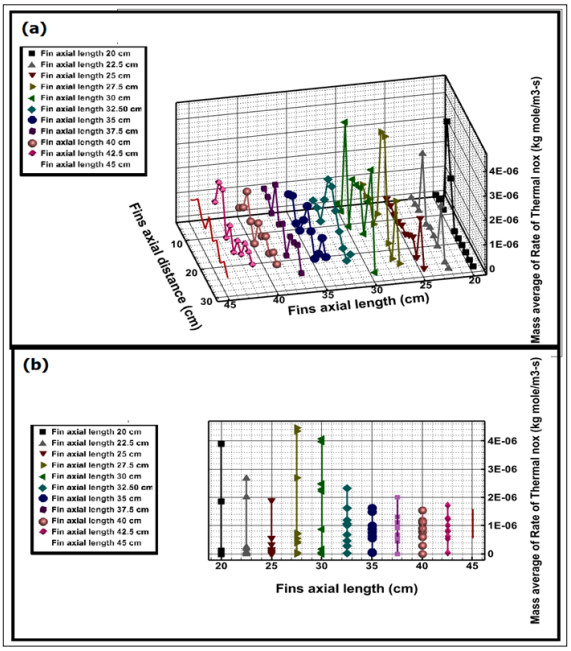

Figure 9: Mass average of the rate of thermal no-formation: (a) Mass average of the rate of thermal no-formation versus fins axial length and fins axial distance and (b) Mass average of the rate of thermal no-formation versus fins axial length

Although NOx could be found pretty early in the flame zone, the production of prompt NOx occurs in less quantity than the production of thermal NOx (Lefebvre and Ballal, 2010)[36]. Prompt NOx generates a more noteworthy effect on the generation of NOx for lean premix combustion. Figure. 10 shows the mass average of the rate of prompt no-formation in the entire burner control volume for reaching the premix combustion process (equivalence ratio=0.9). Figure. 10(a) presents the calculated low prompt no-formation rate (1.35E-012-6.652E-10) *g mole*/(m^3-*s*). As can be seen, when the increase in fin's axial length is smaller than 20 cm and fin axial distance is smaller than 7.5 cm, the minimum values a mass average of rate of prompt no-formation increased. For burner with fins axial distance smaller than 7.5 cm and fins axial length lower than 32.5 cm, the value of Mass average of the rate of prompt no-formation is equal to 6.13E-10 *g mole*/(m^3-*s*). For the case of the burner without fin blades, the value of the mass average of the rate of prompt no-formation is 6.369E-10 k*g mole*/(m^3-*s*). Also, for the burner model with a fin axial length of 32.5 cm and a fin axial distance of 7.5 cm, the mass average of the rate of thermal no-formation is 6.13E-10 k*g mole*/(m^3-*s*) (Figure. 9b).

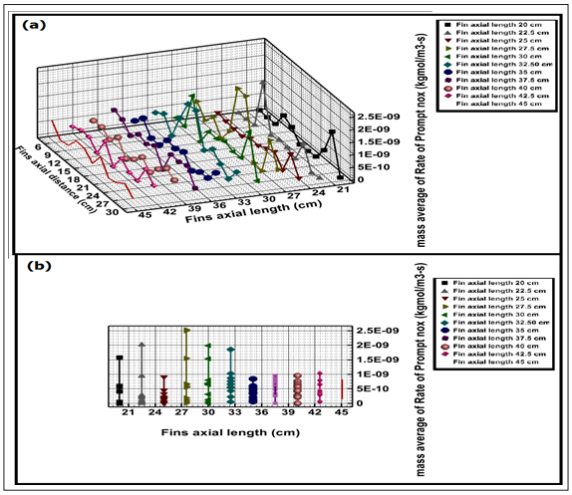

Figure 10: Mass average of the rate of prompt no-formation: (a) Mass average of the rate of prompt no-formation versus fins axial length and fins axial distance and (b) Mass average of the rate of prompt no-formation versus fins axial length

Nox Parts Per Million (Ppm)

In the combustion process, nitrogen oxides (NOx) are generated by reacting between atmospheric nitrogen and oxygen. Generally, nitrogen oxides refer to the sum of the concentrations of 3 terms: either nitrogen dioxide and nitric oxide (NO) or nitrous oxide (NO_2). In the combustion of fuel gases, the air level dilutes the NOx percentage. Therefore, many authorities have chosen a standardized flue gas oxygen reading for which NOx readings are corrected. Generally, NOx is measured by an instrument in ppm. This parameter is calculated using the combustion outlet's fluid flow output [37]. Figure 11 shows the Nitrogen oxide concentration (ppm) at the burner outlet related to the fins axial length and fins axial distance. The decline in NOx concentration can be related to the warm instrument of the nitrogen oxides arrangement, which is essentially related to temperatures lower than 1400°C [38]. Also, the NOppm is computed from Eq. (5), which is the dry ppm. Therefore, the value is normalized by removing the water mole fraction in the dominator.

$$NOppm = \frac{NO\ mole\ fraction \times 10^6}{1 - H_2O\ mole\ fraction} \quad (5)$$

According to Figure. 11(a), the 31.96 ppm value of the combustion chamber was extracted for the case. Here, the fin axial length is 32.5 cm, and the fin axial distance is 7.5 cm. Also, the lowest concentration (i.e., 0.193 ppm) is obtained for the case where the fin axial length is 25 cm and the fin axial distance is 12.5 cm. For the case of a burner without inserting a solid body, the NO_{ppm} is 48.17443. Based on the values in Figure. 11(b), a 33.66% reduction in NO_{ppm} was calculated for the selected model (fin axial length is 32.5 cm and fin axial distance is 7.5 cm).

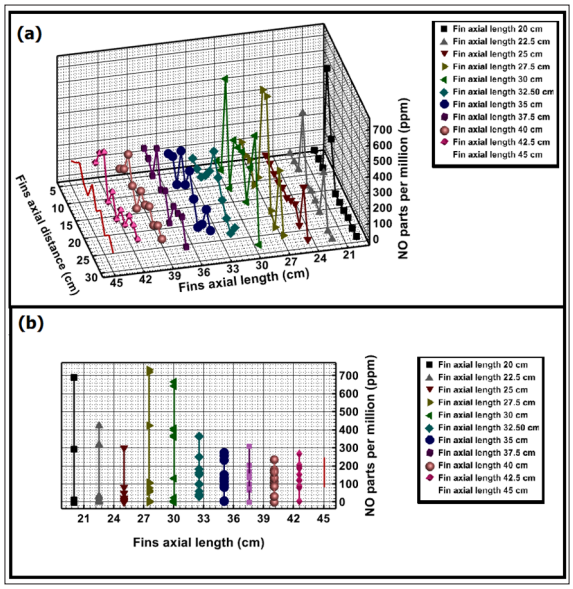

Figure 11: Nitrogen oxide concentration (ppm) at the outlet of the burner: (a) Nitrogen oxide concentration versus fins axial length and fins axial distance and (b) Nitrogen oxide concentration versus fins axial length

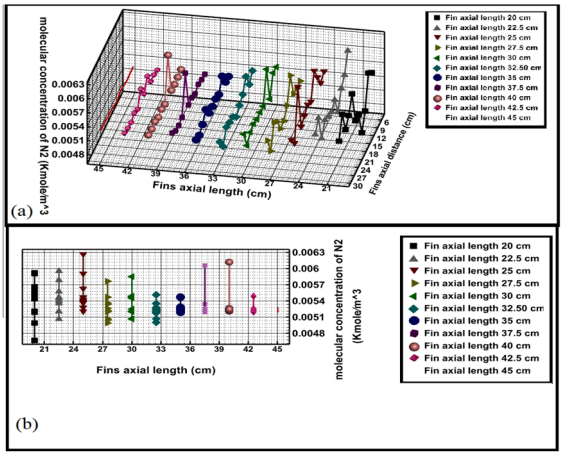

Figure 12: The molecular concentration of N_2 at the outlet of the burner: (a) Molecular concentration of N_2 versus fins axial length and fins axial distance and (b) Molecular concentration of N_2 versus fins' axial length

Molecular Concentration Of N_2

From the view of the air composition, the comparatively high concentration of N2 in the outlet of the burner is the main reason for the decline in NOx emissions [39]. Figure. 12 illustrates the molecular concentration at the burner outlet in numerical simulation and the surrounding environment through the combustion chamber exit. Based on NOx emission results in Figure. 11, the molecular concentration at the outlet of the burner is shown in Figure. 12. This figure shows the variables of fins' axial length and fins' axial distance. The molar concentration for the model with fins axial length of 32.5 cm and fins axial distance of 7.5 cm is equal to 0.005206317 Figure. 12(b). For the model of a burner without inserting a solid body, the molar concentration at the outlet of the burner is 0.022 k mole/m3. Therefore, if the combustion chamber is used with the fin fan blade, the pollution of nitrogen compounds in the combustion process is much less (Figure. 12a)[40].

Conclusion

This research investigates the effects of inserting an aerodynamic solid body with the shape of a 7 7-fin fan blade in the combustion chamber flame region. Also, it discusses the impact of variable fin length and variable distance from the bluff body along the centerline on the combustion chamber temperature flow field and NOx. According to the results, inserting a solid body in the combustion chamber is an effective method for redistribution of temperature field and NOx reduction compared to the ordinary combustion chamber without inserting a solid body. The suitable values of fin length and fin distance of the inserting solid from the bluff body in the combustion chamber flow field are important for increasing the maximum efficiency and NOx reduction from the out-flow combustion chamber. Under the same conditions and related to the ordinary combustion chamber without inserting a solid body, the efficiency of the combustion chamber for inserting a solid body with an axial fin length of 32.5 cm and fin axial distance of 7.5 cm has improved by 2%. Also, a decrease of about 33.66% in the value of NOx (in ppm) was calculated for the selected model. The NOx produced by inserting an aerodynamic solid body is less than that of the non-use of inserting a solid body burner during the combustion process. The combustion peak temperature decreases, and the concentration increases at the outlet where the solid body combustion chamber is inserted. Based on the previous conclusions, inserting an aerodynamic solid body with suitable dimensions is important for NOx production and influence. Installing the solid body in the cylindrical ordinary burner is not very difficult. However, gas pollution reduction is important in producing natural gas, and inserting an aerodynamic solid body is an important way to reduce NOx. For future research, we will carry out deeper research on the other dimension parameters, such as the aerodynamic shape and position of inserting solid body. The research results will be used to achieve a greater reduction of emissions of pollutants. Furthermore, they can be used to adapt the standards for the new manufacturing combustion chambers with more advanced global pollutant standards and stricter regulations.

References

1. Nandhini R, Sivaprakash B, Rajamohan N. Waste heat recovery at low temperature from heat pumps, power cycles and integrated systems–Review on system performance and environmental perspectives. Sustainable Energy Technologies and Assessments. 2022. 52: 102214.
2. Wang X, Li C, Lam Ch, Subramanian K, Qin Z-H, et al. Emerging waste valorisation techniques to moderate the hazardous impacts, and their path towards sustainability. Journal of hazardous materials. 2022. 423: 127023.

3. Gao X, Duan F, Lim Sc, Yip Ms. NOx formation in hydrogen–methane turbulent diffusion flame under the moderate or intense low-oxygen dilution conditions. Energy. 2013. 59: 559-569.
4. Nabi Mn. Theoretical investigation of engine thermal efficiency, adiabatic flame temperature, NOx emission and combustion-related parameters for different oxygenated fuels. Applied Thermal Engineering. 2010. 30: 839-844.
5. Chen Z, Li Z, Zhu Q, Jing J. Gas/particle flow and combustion characteristics and NOx emissions of a new swirl coal burner. Energy. 2011. 36: 709-723.
6. Gentile G, debiagi PE, cuoci A, frassoldati A, faravelli T, et al. A CFD model for biomass flame-combustion analysis. Chemical Engineering Transactions. 2016. 50: 49-54.
7. Jegla Z, Vondál J, Hájek J. Standards for fired heater design: An assessment based on computational modelling. Applied Thermal Engineering. 2015. 89: 1068-1078.
8. Stefanidis GD, Merci B, Heynderickx GJ, Marin GB. CFD simulations of steam cracking furnaces using detailed combustion mechanisms. Computers & chemical engineering. 2006. 30: 635-649.
9. Pitsch H, Steiner H. Scalar mixing and dissipation rate in large-eddy simulations of non-premixed turbulent combustion. Proceedings of the Combustion Institute. 2000. 28: 41-49.
10. Pitsch H, Steiner H. Large-eddy simulation of a turbulent piloted methane/air diffusion flame (Sandia flame D). Physics of fluids. 2000. 12: 2541-2554.
11. Pitsch H, Ihme M. An unsteady/flamelet progress variable method for LES of nonpremixed turbulent combustion. 43rd AIAA Aerospace Sciences Meeting and Exhibit, 2005. 557.
12. Ihme M, Pitsch H. Modeling of radiation and nitric oxide formation in turbulent nonpremixed flames using a flamelet/progress variable formulation. Physics of Fluids. 2008. 20.
13. Peters N. Laminar diffusion flamelet models in non-premixed turbulent combustion. Progress in energy and combustion science. 1984. 10: 319-339.
14. Ilbas M, Yilmaz I, Veziroglu Tn, Kaplan Y. Hydrogen as burner fuel: modelling of hydrogen–hydrocarbon composite fuel combustion and NOx formation in a small burner. International journal of energy research, 2005. 29: 973-990.
15. Saponaroa A, Senneca O. Cfd modeling: a powerful tool for high efficiency burner design. European conference on industrial furnaces and boilers (INFUB-12), 2020.
16. Rago Gd, Rossiello G, Dadduzio R, Giani T, Saponaro A, et al. CFD analysis of a swirl stabilized coal combustion burner. Energy Procedia. 2018. 148: 703-711.
17. Torresi M, Fornarelli F, Fortunato B, Camporeale SM, Saponaro A. Assessment against experiments of devolatilization and char burnout models for the simulation of an aerodynamically staged swirled low-NO x pulverized coal burner. Energies. 2017. 10: 66.
18. Cala O, Meriño L, Kafarov V, Saavedra J. Effect of the composition of the refinery gas on the characteristics of the combustion process. Engineering Journal University of Medellín. 2013. 12: 101-111.
19. Cala Parra O. Determination of an energy efficiency index for combustion processes of gas mixtures in refinery. M. sc Thesis. Universidad Industrial de Santander, Bucaramanga, Colombia. 2014.
20. Aminian J, Shahhosseini S, Bayat M. Investigation of temperature and flow fields in an alternative design of industrial cracking furnaces using CFD. 2010.
21. Boggavarapu P, Ray B, Ravikrishna R. Thermal efficiency of LPG and PNG-fired burners: Experimental and numerical studies. Fuel. 2014. 116: 709-715.
22. Abdelaal M. Redistribution of flame temperatures to reduce thermal no-formation. Journal of Engineering and Applied Science. 2002. 49: 513-528.
23. Kazim MNFM, Rasani R, Nuawi MZ, Harun Z, Hau YK, et al. Analysis of wake region behind bluff body for piezoelectric energy harvester. Journal of Advanced Research in Fluid Mechanics and Thermal Sciences. 2019. 55: 249-263.
24. Deng F, Zhao M, Qin S, Wang Z, Xie Y, et al. Numerical simulation study on the dynamics of bluff-body flames under oxygen-lean conditions. Energies. 2023. 17: 142.
25. Pitsch H. Large-eddy simulation of turbulent combustion. Annu. Rev. Fluid Mech, 2006. 38: 453-482.
26. Kurenkov A, oberlack M. Modelling turbulent premixed combustion using the level set approach for Reynolds averaged models. Flow, turbulence and combustion. 2005. 74: 387-407.
27. Lalmi D, Hadef R. 2017. Numerical study of the swirl direction effect at the turbulent diffusion flame characteristics. International Journal of Heat and Technology. 35: 520-528.
28. Lalmi D, Hadef R. Influence of direction of rotation of the swirl at the turbulente diffusion flame proprieties. 2017 International Conference on Green Energy Conversion Systems (GECS). 2017. 1-8.
29. Lalmi D, Hadef R. Numerical simulation of co-and counter-swirls on the isothermal flow and mixture field in a combustion chamber. Advances and Applications in Fluid Mechanics. 2015. 18: 199.
30. Syred N. Beer J. Combustion in swirling flows: a review. Combustion and flame. 1974. 23: 143-201.
31. Pierce C, Moin P. Large eddy simulation of a confined coaxial jet with swirl and heat release. 29th AIAA, Fluid Dynamics Conference. 1998. 2892.
32. Pierce CD, Moin P. Method for generating equilibrium swirling inflow conditions. AIAA journal. 1998. 36: 1325-1327.
33. Merkle K, Haessler H, Büchner H, Zarzalis N. Effect of co-and counter-swirl on the isothermal flow-and mixture-field of an airblast atomizer nozzle. International Journal of Heat and Fluid Flow. 2003. 24: 529-537.
34. Kumar R, Sood S. Combined influence of fluctuations in the temperature and stretching velocity of the sheet on MHD flow of Cu-water nanofluid through rotating porous medium with cubic auto-catalysis chemical reaction. Journal of Molecular Liquids. 2017. 237: 347-360.
35. Kumar R, Sood S, Sheikholeslami M, Shehzad SA. Nonlinear thermal radiation and cubic autocatalysis chemical reaction effects on the flow of stretched nanofluid under rotational oscillations. Journal of colloid and interface science. 2017. 505: 253-265.
36. Lefebvre AH, Ballal DR. Gas turbine combustion: alternative fuels and emissions, CRC press. 2010.
37. Chen L, Xu Y, Tian S, Lu H. Numerical Simulation Study of Combustion under Different Excess Air Factors in a Flow Pulverized Coal Burner. Processes. 2024. 12: 1607.

38. Marin O, Chatel-Pelage F, Ghani M, Perrin N, Carty R, et al. Low-oxygen enrichment in coal-fired utility boilers. Twenty-eighth International Technical Conference on Coal Utilization and Fuel Systems. 2003.
39. Rassai N, Boutammachte N. Environmental impacts analysis of Moroccan olive cake combustion in Stirling motor cogeneration system: Case study. Heliyon. 2024. 10.
40. Fu Z, Gao H, Zeng Z, Liu J, Zhu Q. Generation characteristics of thermal NOx in a double-swirler annular combustor under various inlet conditions. Energy. 2020. 200: 117487.